Erik P. Schartner, Stephen C. Warren-Smith, Linh V. Nguyen, Dale Otten, Zheng Yu, David G. Lancaster and Heike Ebendorff-Heidepriem

Single-peak fiber Bragg gratings in suspended-core optical fibers

Optics Express, 2020; 28(16):23354-23362

DOI: http://dx.doi.org/10.1364/OE.397537

Research Article | Vol. 28, No. 16 / 3 August 2020 / Optics Express 23354
Optics EXPRESS

Single-peak fiber Bragg gratings in suspended-core optical fibers

ERIK P. SCHARTNER,[1,2,*] STEPHEN C. WARREN-SMITH,[1,2] LINH V. NGUYEN,[1,3] DALE OTTEN,[3] ZHENG YU,[1] DAVID G. LANCASTER,[3] AND HEIKE EBENDORFF-HEIDEPRIEM[1,2]

[1]*Institute for Photonics and Advanced Sensing and School of Physical Sciences, The University of Adelaide, Adelaide, SA 5005, Australia*
[2]*ARC Centre of Excellence for Nanoscale BioPhotonics, The University of Adelaide, Adelaide, SA 5005, Australia*
[3]*UniSA STEM and Future Industries Institute, University of South Australia, Mawson Lakes, SA 5095, Australia*
[*]*erik.schartner@adelaide.edu.au*
https://researchers.adelaide.edu.au/profile/erik.schartner

Abstract: Femtosecond laser inscribed fiber Bragg gratings in pure-silica suspended-core optical fibers have previously been demonstrated as a promising platform for high temperature sensing. However, the density of gratings that could be written on a single fiber was limited by undesired reflections associated with higher order modes in these high numerical aperture fibers. This resulted in a complex, broadband reflection spectrum with limited multiplexing capability. In this work we utilize modifications to the fine structure of the suspended core optical fibers to fine tune the relative confinement loss of the optical fiber modes, thus reducing the contribution from such higher order modes. The effects of these changes on mode propagation are modeled, giving a range of fibers with different confinement loss properties which can be tailored to the specific length scale of a desired application. We achieve single-peak reflections from individual fiber Bragg gratings, significantly improving performance for multipoint sensing and demonstrate this technique by writing 20 gratings onto a single fiber.

1. Introduction

Fiber Bragg gratings (FBGs) have found common use for structural health monitoring, with applications including multipoint temperature sensing [1]. Typical FBGs written in conventional core/clad single-mode fibers (SMF) are limited to temperatures below 500°C, above which thermal annealing of the grating structure removes the refractive index modulations that make up the grating [1,2]. Specialty fibers or grating writing techniques can expand this operating range, such as regenerated FBGs [3,4], chiral gratings [5], or femtosecond laser written gratings [6], allowing for sensing up to the order of 1100-1295°C. Sapphire crystal optical fibers have also shown promise for sensing above this temperature range due to their increased material stability at higher temperatures. Practical sensors based on sapphire however have been impaired by both the high loss of the fibers, and the broad FBG reflection peaks due to the large number of guided-modes supported by the coreless fiber [7].

An alternative approach is the use of microstructured silica optical fibers, in particular the suspended core fiber (SCF) geometry that consists of three evenly spaced holes in the cross section, creating a structure where the light confinement comes from the glass/air index contrast (Fig. 1). SCFs have found a number of applications in recent years, primarily for biological and chemical sensing [8,9] due to the high capture of fluorescent light by the evanescent field [10]. Previous work on SCFs has shown that a variety of sensing methodologies can be employed using these fibers, with temperature sensing being demonstrated in particular either through

#397537 https://doi.org/10.1364/OE.397537
Journal © 2020 Received 13 May 2020; revised 25 Jun 2020; accepted 1 Jul 2020; published 22 Jul 2020

Optics EXPRESS

multimode interference [11] or femtosecond laser written type II damage gratings [12]. These gratings have also been demonstrated on exposed core fibers [13,14], allowing for direct contact with the liquids or gases of an external environment for refractive index based sensing. For temperature sensing applications the enclosed SCF geometry also provides a more robust option, as the core is protected from contamination from the external environment.

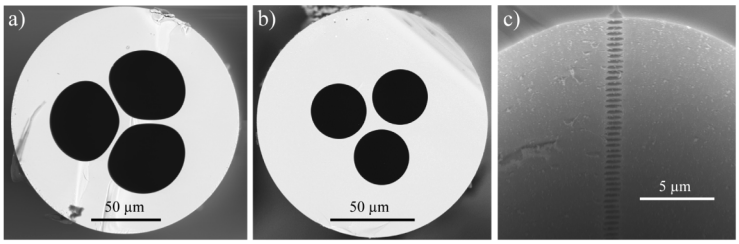

Fig. 1. Scanning electron microscope (SEM) images of (a) thin strut (2.7 µm), (b) thick strut (4.3 µm) SCFs and (c) femtosecond laser ablation grating on the SCF core surface.

Our previous work in the application of SCFs to high temperature sensing demonstrated the use of these fibers up to 1300°C for short time durations [12], and up to 1150°C for longer durations [15]. The suitability for high temperature operation comes from using un-doped high-purity silica glass, thus avoiding dopant diffusion at high temperature. Unlike photosensitive FBGs, the SCF FBG is based on the irreversible physical removal of material using the femtosecond laser ablation process. However, a notable limitation of the SCF is that the large core size, with thin struts, supports multiple guided transverse optical modes. FBGs written onto the core of the fiber therefore reflect several resonant peaks, corresponding to these higher order modes (HOMs), across a bandwidth of 8-12 nm. This bandwidth requirement puts a fundamental limit on the possible wavelength separation of gratings written within the same fiber before overlap or interaction between the peaks is observed between the gratings. The inclusion of HOMs also adds to the complexity of analyzing the peak positions, as an algorithm is required to determine which of the peaks should be tracked, and leads to inaccuracies if the peak tracking switches between modes within the fiber [16]. For example, our previous study was limited to a maximum of three FBGs in a single fiber [12].

One possibility for reducing the modal content of the fibers is to physically reduce the size of the core, with literature demonstrating cores as small as 800 nm in silica [17], or 400 nm in soft-glass [18], at which point the fiber is inherently single-moded. However, the typical feature size of the femtosecond laser ablation points are in the order of 1 µm [12] and thus writing the grating would cause significant damage to the core, as previously observed when writing FBGs in a 2.7 µm core diameter exposed-core optical fiber [14]. Additionally, when the core size is significantly different to that of the SMF lead-in fibers high splice losses are observed [14].

An alternative approach for reducing the transverse mode content is the leaky-mode fiber concept, which allows for larger core sizes while still maintaining effectively single mode guidance [19–21]. In these fibers the confinement loss of the HOMs in the fiber is designed to be higher than that of the fundamental mode. Over a sufficient length, the energy transported by the HOMs is lost into the fiber cladding and the fiber becomes effectively single-moded.

Here we exploit this technique to achieve single-peak reflections from FBGs in suspended-core optical fiber. By controlling the strut thickness (through modification of the internal hole sizes) in the SCF, we tune the relative confinement loss of the HOMs compared to the fundamental mode of the fiber. We demonstrate that fibers can be drawn with preferential losses of the fundamental mode relative to the HOMs appropriate to specific applications allowing single-peak reflection FBGs to be formed. Numerical analysis of the confinement losses in these geometries shows that effective single mode behavior can be achieved for anywhere between relatively short (<1 m) to

Optics EXPRESS

relatively long (>20 m) lengths of the lead-in fiber to the FBG sensing element. We then show the practical usage of these single-peak FBGs by writing 20 gratings into a single fiber with a significantly higher spectral density than was previously possible using similar fibers without a tailored geometry.

2. Fabrication methods

2.1. Suspended-core optical fiber

Fabrication of the SCFs was based on existing techniques described in detail in previous work [12,22]. Preliminary finite element modeling (FEM) was performed in COMSOL Multiphysics to determine the target geometry (see Sec. 3.2). Fused silica glass rods with a length of 150 mm (Heraeus LWQ/HSQ300) were drilled using an ultrasonic mill to create the triangular pattern of holes that comprise the voids in the structure (3×2.8 mm holes with 0.4 mm spacing between adjacent holes). Preforms were drilled from both ends to maximize the usable length.

The preform was then drawn to fiber using a 6 m draw tower, controlling the pressure applied to the three holes and the outer diameter of the fiber to create the desired structure. Lower pressures gave less inflation of the structure, resulting in thicker, shorter struts with a similar core diameter. The difference between the core diameters of the thin and thick strut versions of the fiber when controlling parameters was only 8% (9.8 µm and 10.5 µm for the thin and thick strut fibers, respectively) as seen in Fig. 1 below.

2.2. Fiber Bragg gratings

The SCFs were spliced to conventional SMF28E fiber for ease of integration with testing equipment using a Fujikura FSM-100P arc splicer. This allowed spectra to be recorded using commercial FBG interrogators (Micron Optics). Due to the mode mismatch between the two fibers measured splice losses were approximately 2-3 dB. Minimal deformation of the structure was observed during splicing, with a comparable transmitted power before and after splicing.

FBGs were written into the SCFs using a method based on that described previously [12,15]. The fibers were first mounted in a groove on an aluminum block, taking care that the fiber lay flat in the groove with no curvature of the fiber out of the groove or rotation of the fiber along the length. The optical fiber was then orientated using a rotation mount such that one hole faced vertically out from the block and thus facing towards the femtosecond laser beam path.

Two femtosecond laser systems were used in this work. The results in Sec. 3.1 were obtained using a 800 nm femtosecond laser (Hurricane Ti:Sapphire) operating at a repetition rate of 100 Hz with the pulses focused onto the fiber core surface using a 40× microscope objective (see [12] for more details). The results in Sec. 3.3 were obtained using a wavelength-doubled (524 nm), ultra-fast laser (IMRA DE0210) with pulse duration < 250 written at 1 kHz using a pulse picker (see [15] for more details). In both cases the grating length was set to 2 mm for each FBG, with the FBGs written by translating the stage along a line between two points along the surface of the fiber core. The speed of the stage was adjusted to create a grating pitch the order of 1 µm such that second order FBG reflections occurred at approximately 1500 nm and tuned according to the exact wavelength desired.

The primary difference between the two systems was the pulse energy required in order to operate slightly above the ablation threshold, which was approximately 100 nJ for the 524 nm system and 400 nJ for the 800 nm system. Otherwise, FBGs written using both methodologies were qualitatively similar when written into SCF with same geometries, especially with respect to the expression of HOM reflections.

Optics EXPRESS

3. Results

3.1. Experimental

Example structures of both thin and thick strut SCFs are shown in Fig. 1(a) and Fig. 1(b), respectively. In this work we define the strut thickness as the thickness at the smallest point along the strut (the waist), averaged over the three struts.

FBGs were then written into both thin strut (2.7 μm thickness) and thick strut (4.3 μm thickness) fibers, which had core sizes of 9.8 μm and 10.5 μm, respectively. An SEM image of a typical surface-based femtosecond laser ablation grating written in this work is shown in Fig. 1(c). Example reflection spectra for these fibers are shown in Fig. 2 below.

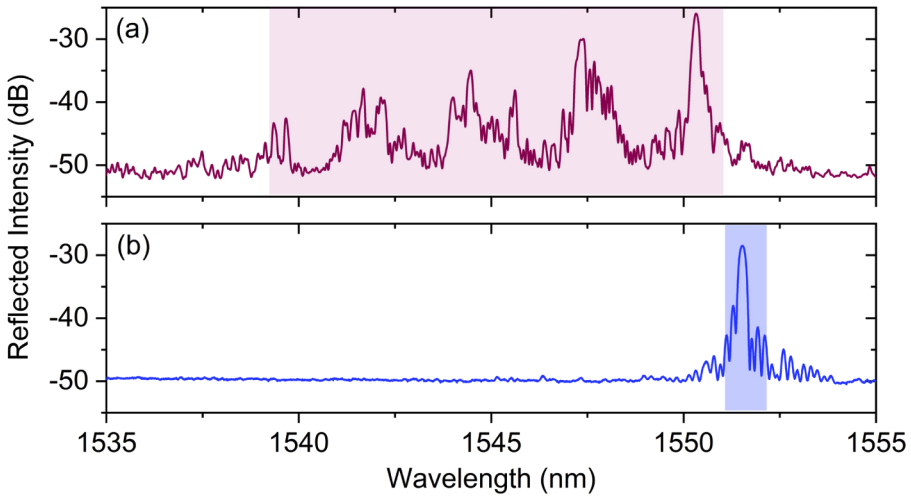

Fig. 2. FBG reflection spectra. (a) SCF with 2.7 μm strut width resulting in a 11.6 nm reflected spectral bandwidth. (b) SCF with 4.3 μm strut width resulting in a 1.2 nm reflected spectral bandwidth. The shaded regions indicate the spectral width of the reflected peak that is a minimum of 5 dB over the background. Spectra were measured using a Micron Optics sm125 FBG interrogator (bandwidth: 1510-1590 nm).

To quantify the bandwidth required for a single sensing point, we consider the spectral bandwidth of the reflection signal from an FBG on both a thin and thick strut fiber. By comparing the reflection spectra for the two fibers and taking the bandwidth to be the spectral width required to contain all peaks that are at least 5 dB above the background, we can examine the performance of the two example strut thicknesses. Applying this criterion to the spectra in Fig. 2 we see that sensors on the thin strut fiber [geometry shown in Fig. 1(a), spectra in Fig. 2(a)] require a total spectral bandwidth of 11.6 μm, while sensors on the thick strut fiber [geometry shown in Fig. 1(b), spectra in Fig. 2(b)] require a total spectral bandwidth of only 1.2 μm. The spectral width of the individual peaks of the two fibers is comparable (approximately 0.2 nm full width at half maximum), with the primary difference in the FBG spectra being the suppression of the HOMs for the thick strut fiber.

3.2. Numerical simulations

While the thicker strut SCFs shown here can successfully suppress the HOM content of the FBG reflection, this comes at the cost of increased loss of the fundamental mode. For example, fundamental mode losses of 1 dB/m would restrict the fiber length to 10-15 m before the reflected signal is too weak to be observed over the background reflections from the fiber.

Optics EXPRESS

To examine this in more detail, SEM images of the fiber structures were imported into a commercial finite element analysis package (COMSOL Multiphysics) to analyze the confinement loss of both the fundamental mode and HOMs guided within the fiber. The results are shown in Fig. 3 below.

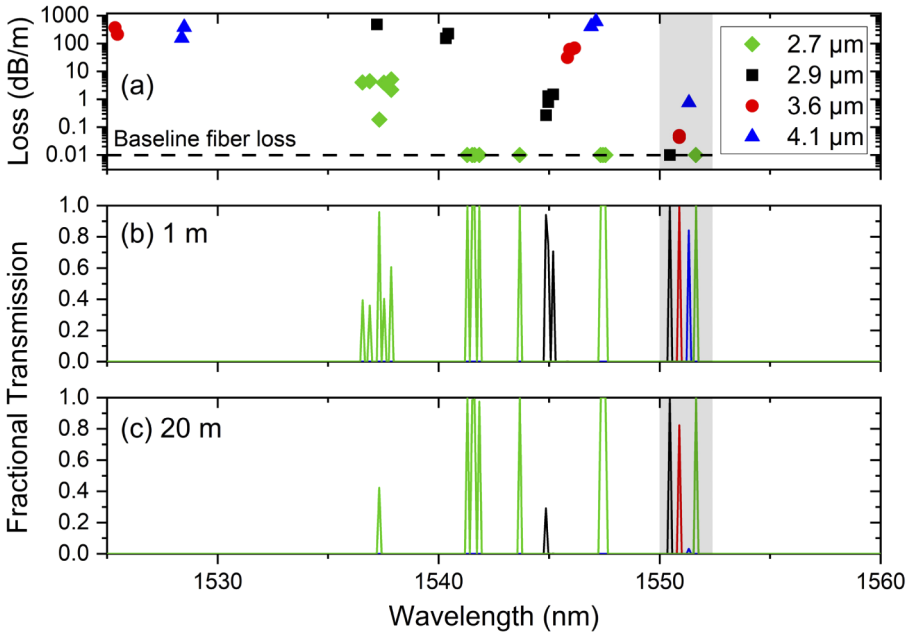

Fig. 3. (a) Calculated confinement loss based on SEMs of SCFs that were drawn with varying strut thickness. Here the effective index of the mode has been converted to an equivalent Bragg wavelength for a second order grating with a pitch of 1.077 μm. Modes with losses above 1000 dB/m have been removed and modes with losses below 0.01 dB/m have been set to 0.01 dB/m as this is the approximate baseline fiber loss for our SCFs. (b, c) Calculated fractional transmission of light for each of the modes shown in (a) for both 1 m (b) and 20 m (c) lengths. Here all modes are assumed to create a Bragg peak with an intensity of 1 and the intensity at the proximal end of the fiber is then calculated based on the loss of the individual modes. Shaded regions highlight the fundamental mode of each of the modeled geometries

Figure 3(a) shows the results of the simulations of the realized fiber geometries applied to fibers with strut thicknesses ranging from 2.7 to 4.1 μm. To better show the relationship between the modal content of the fiber and the expected performance of the fiber with an included FBG, the effective index (n_{eff}) of the fiber has been converted to an effective Bragg wavelength (λ_B) reflection using $m\lambda_B = 2\Lambda n_{eff}$, where the pitch ($\Lambda$) was set to 1.077 μm such that a second order ($m = 2$) reflection from the fundamental mode occurs at approximately 1550 nm.

The results show that the fundamental mode loss increases with increasing strut width, as expected. Here we have also set a "minimum practical loss" of the fibers to 10 dB/km, as modes with a confinement loss lower than this will be dominated by scattering or material losses.

The important parameter to be considered from this plot is the difference between the loss of the fundamental mode and that of the HOMs guided within the fiber. If this difference between the modes is small, it becomes challenging to suppress HOMs without also significantly affecting the strength of the fundamental peak. A fiber with strut thickness of 2.7 μm clearly shows a large number of modes with low loss, while the 2.9 μm strut thickness fiber shows a higher order mode with only 26× suppression between the fundamental and the next HOM. Fibers with strut

Optics EXPRESS

thicknesses ranging between 3.6-4.1 μm show at least 380× suppression, with fundamental mode losses ranging from 0.05-1.4 dB/m.

To understand how the modal losses in Fig. 3(a) translate to the resultant FBG spectra, the losses were converted to a fractional transmission by considering the confinement loss from a peak with an intensity of one for each mode found by the FEM model. The confinement loss of a corresponding mode was then applied to fiber lengths of 1 m [Fig. 3(b)] and 20 m [Fig. 3(c)]. Comparing Figs. 3(b) and 3(c) we see that for the thin strut fibers the increase in length changes the mode structure, while for the thickest strut fibers shown here the confinement loss of the fundamental mode starts to become significant. For the 4.1 μm strut fiber there is effectively no reflection peak after transmitting through 20 m of fiber as even the fundamental mode has been lost. We note here that the thicker strut fibers (> 2.9 μm) all show effectively single mode behavior, with only a single peak observed after even a moderate lead-in length of 1 m.

To better understand the effects of the strut thickness over a broader range of fiber geometries we simulated variation in the strut thickness for three different core sizes (6 μm, 8 μm, and 10 μm) by simplifying the hole geometry to a circle and changing the diameter of the holes. The resultant losses for both the fundamental and first HOM are shown in Fig. 4(a) with the corresponding ratio between these two values is shown in Fig. 4(b). These results demonstrate that the appropriate loss of the fiber, and required suppression ratio, can be obtained across a wide variety of core sizes. Figure 4 also provides important information on the fabrication tolerance for achieving both the required suppression ratio of the HOMs and loss of the fundamental mode. For example, for a 10 μm core diameter fiber where a HOM loss of > 10 dB/m is required but

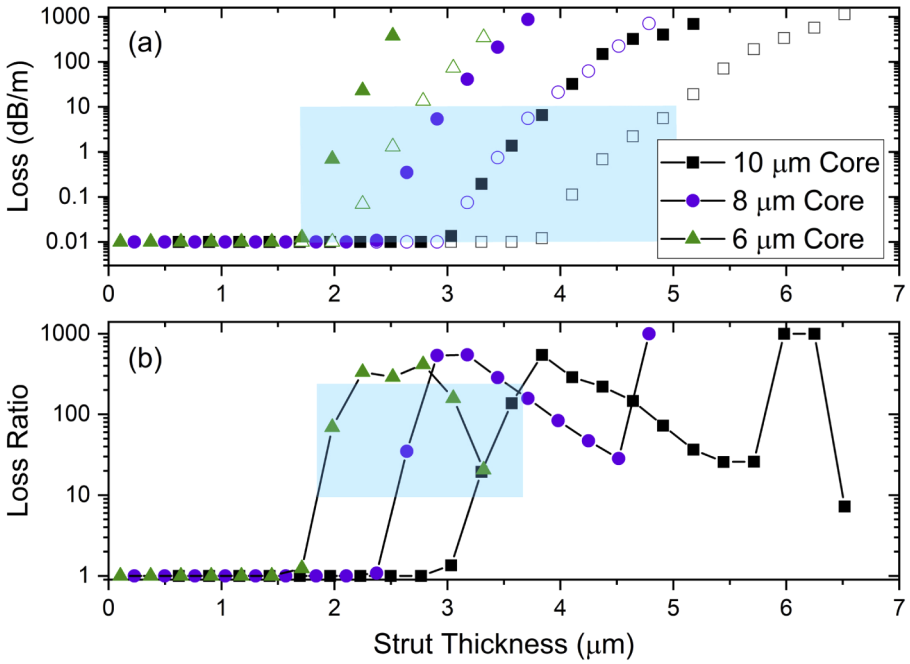

Fig. 4. (a) Loss for three different core sizes (6 μm, 8 μm, and 10 μm) as a function of strut thickness when varying the diameter of the holes. Open symbols show the loss of the fundamental mode and the closed symbols show the loss of the first HOM. Blue shading shows the approximate region in which the loss of the fiber is within desired operating limits. (b) Ratio between the loss of the first HOM and the fundamental mode. Here the ratio represents the suppression ratio of the fiber, with a higher value representing a larger suppression of the HOM relative to the fundamental.

Optics EXPRESS

with the fundamental mode loss less than 0.1 dB/m (i.e. loss ratio > 100), then the fabricated strut thickness must lie between approximately 3.9 and 4.1 μm.

3.3. Demonstration of multiple fiber Bragg gratings

As a proof-of-concept demonstration for multi-grating sensors, a series of 20 × 2 mm long gratings were written into a thick-strut SCF (strut thickness 3.2 μm, core diameter 8.5 μm), with the results shown in Fig. 5. The wavelength spacing between adjacent gratings was chosen as 6.4 nm, which corresponds to a 500°C temperature induced spectral shift from ambient. In comparison, a temperature sensor based on the thin strut fiber with the reflection spectra shown in Fig. 2(a) would require an 11.6 nm bandwidth in addition to the 6.4 nm spacing for the potential temperature change (18 nm total). This spectral requirement is overlaid on the 20 grating spectra in Fig. 5, shaded in blue, indicating approximately three times improvement in multiplexing capability for the thicker strut fiber.

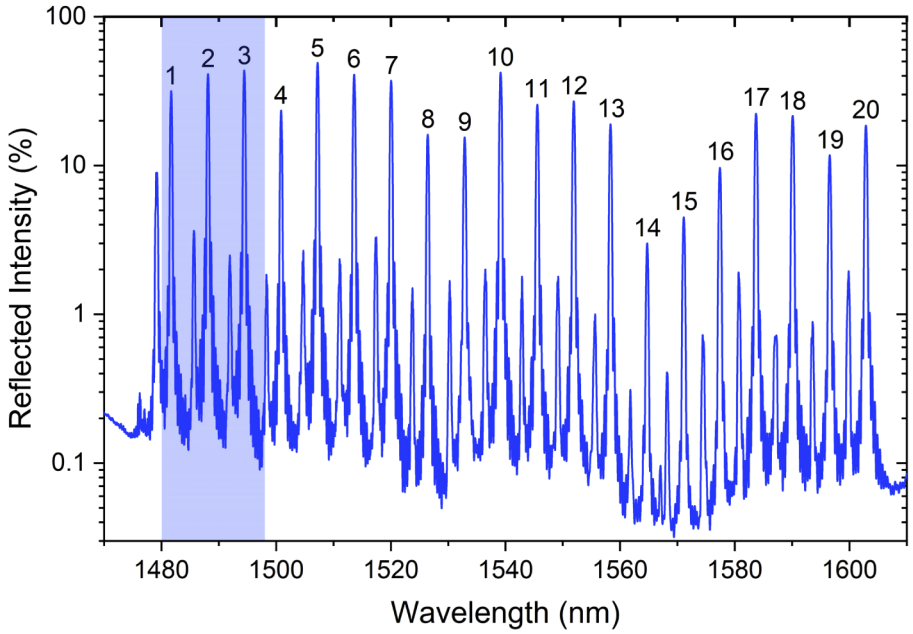

Fig. 5. Reflection spectrum for a thick strut SCF (strut thickness 3.2 μm, core diameter 8.5 μm) with 20 FBGs separated spectrally by 6.4 nm each. Absolute reflectivity obtained by comparison to a fiber optic retroreflector (Thorlabs, P5-SMF28ER-P01-1). The spectral bandwidth requirement for fibers with thin struts is shaded in blue [11.6 nm from Fig. 2(a) plus 6.4 nm, corresponding to a 500°C temperature induced spectral shift from ambient]. The peaks corresponding to the fundamental mode are labelled 1-20, in order of distance from the FBG interrogator (Micron Optics si255 FBG interrogator, bandwidth: 1460-1620 nm). Data originally presented in [23].

The reflected peaks in Fig. 5 show that despite some variability between the gratings due to imperfect alignment of the femtosecond light onto the core of the fiber, and minor fiber irregularities, all 20 peaks can be clearly differentiated. Minimal broadband loss is induced even with a large number of gratings on a single fiber, with a linear fit applied to the peak heights yielding an average dual-pass loss of 0.31 dB per grating.

The individual peaks show clean spectral features, with effectively one single peak per FBG. It can be seen that in between the fundamental mode reflection peaks (numbered) that there are peaks approximately 10 dB lower in reflectivity, which correspond to a second order mode.

Optics EXPRESS

While undesirable, we have nevertheless suppressed higher order mode content such that these peaks can be readily ignored using peak tracking techniques due to being significantly lower in reflectivity compared to adjacent peaks.

4. Discussion and conclusions

We have demonstrated a new thick-strut variant of SCFs to obtain single-peak reflections from femtosecond laser-ablation written FBGs. Tailoring the fiber geometry allows for effectively single peak FBG reflection spectra through the use of thicker struts to increase the confinement loss of HOMs. This alteration to the geometry allows for increased wavelength division multiplexing capacity and simpler peak tracking algorithms to be used for sensing applications.

Our theoretical results demonstrate that a sufficient HOM suppression ratio can be obtained for a broad range of core diameters, ranging from 6 to 10 μm in this work. Such core diameters allow for splicing with standard single mode optical fibers, thus allow for simple integration with existing interrogation equipment. There are tighter requirements for the strut thickness, with the tolerance being approximately 0.2 μm. However, our experimental results demonstrate that this is readily achievable through active control of the internal fiber pressure during drawing. We have demonstrated this technique by create an FBG sensor with 20 discrete reflection points, a significant improvement on previous work where only three FBGs were written into a fiber over an 80 nm measurement bandwidth.

Our study has focused on the use of femtosecond laser ablation gratings, which hold great potential for temperature sensing in extreme environments. However, this same technique could also be used to create single-peak fiber Bragg gratings in suspended-core fiber for applications that utilize the SCF's ability to facilitate light-matter interactions, such as chemical and biological sensing, lasing, and nonlinear and quantum optics.

Funding

Cooperative Research Centres, Australian Government Department of Industry; University of Adelaide (Ramsay Fellowship); Mitsubishi Heavy Industries; Australian National Fabrication Facility (OptoFab node, SA and Commonwealth funded); SJ Cheesman; ARC (CE1410003, LP150100657).

Acknowledgments

The authors acknowledge Ben Johnston and Martin Ams from Macquarie University for assistance in using the femtosecond laser facility at Macquarie University. The authors acknowledge Alastair Dowler and Evan Johnston for their contribution to the suspended-core optical fiber fabrication.

Disclosures

E.P.S. and S.C.W.S. are directors of HT Sensing Pty Ltd, a company that manufactures optical fiber sensors. HT Sensing Pty Ltd did not contribute to or participate in this research in any way.

References

1. A. Othonos, "Fiber Bragg gratings," Rev. Sci. Instrum. **68**(12), 4309–4341 (1997).
2. B. Lee, "Review of the present status of optical fiber sensors," Opt. Fiber Technol. **9**(2), 57–79 (2003).
3. J. Canning, M. Stevenson, S. Bandyopadhyay, and K. Cook, "Extreme silica optical fibre gratings," Sensors **8**(10), 6448–6452 (2008).
4. D. Barrera, V. Finazzi, J. Villatoro, S. Sales, and V. Pruneri, "Packaged optical sensors based on regenerated fiber Bragg gratings for high temperature applications," IEEE Sens. J. **12**(1), 107–112 (2012).
5. V. I. Kopp, V. M. Churikov, G. Zhang, J. Singer, C. W. Draper, N. Chao, D. Neugroschl, and A. Z. Genack, "Single- and double-helix chiral fiber sensors," J. Opt. Soc. Am. B **24**(10), A48–A52 (2007).
6. C. R. Liao and D. N. Wang, "Review of femtosecond laser fabricated fiber Bragg gratings for high temperature sensing," Photonic Sens. **3**(2), 97–101 (2013).

Optics EXPRESS

7. T. Habisreuther, T. Elsmann, Z. Pan, A. Graf, R. Willsch, and M. A. Schmidt, "Sapphire fiber Bragg gratings for high temperature and dynamic temperature diagnostics," Appl. Therm. Eng. **91**, 860–865 (2015).
8. E. P. Schartner, G. Tsiminis, A. François, R. Kostecki, S. C. Warren-Smith, L. V. Nguyen, S. Heng, T. Reynolds, E. Klantsataya, K. J. Rowland, A. D. Abell, H. Ebendorff-Heidepriem, and T. M. Monro, "Taming the light in microstructured optical fibers for sensing," Int. J. Appl. Glass Sci. **6**(3), 229–239 (2015).
9. T. M. Monro, S. Warren-Smith, E. P. Schartner, A. François, S. Heng, H. Ebendorff-Heidepriem, and S. Afshar V, "Sensing with suspended-core optical fibers," Opt. Fiber Technol. **16**(6), 343–356 (2010).
10. E. P. Schartner, G. Tsiminis, M. R. Henderson, S. C. Warren-Smith, and T. M. Monro, "Quantification of the fluorescence sensing performance of microstructured optical fibers compared to multi-mode fiber tips," Opt. Express **24**(16), 18541–18550 (2016).
11. L. V. Nguyen, S. C. Warren-Smith, H. Ebendorff-Heidepriem, and T. Monro, "Interferometric high temperature sensor using suspended-core optical fibers," Opt. Express **24**(8), 8967–8977 (2016).
12. S. C. Warren-Smith, L. V. Nguyen, C. Lang, H. Ebendorff-Heidepriem, and T. M. Monro, "Temperature sensing up to 1300(C using suspended-core microstructured optical fibers," Opt. Express **24**(4), 3714–3719 (2016).
13. S. C. Warren-Smith and T. M. Monro, "Exposed core microstructured optical fiber Bragg gratings: refractive index sensing," Opt. Express **22**(2), 1480–1489 (2014).
14. S. C. Warren-Smith, R. Kostecki, L. V. Nguyen, and T. M. Monro, "Fabrication, splicing, Bragg grating writing, and polyelectrolyte functionalization of exposed-core microstructured optical fibers," Opt. Express **22**(24), 29493–29504 (2014).
15. S. C. Warren-Smith, E. P. Schartner, L. V. Nguyen, D. E. Otten, Z. Yu, D. G. Lancaster, and H. Ebendorff-Heidepriem, "Stability of grating-based optical fiber sensors at high temperature," IEEE Sens. J. **19**(8), 2978–2983 (2019).
16. D. Tosi, "Review and analysis of peak tracking techniques for fiber Bragg grating sensors," Sensors **17**(10), 2368 (2017).
17. A. S. Webb, F. Poletti, D. J. Richardson, and J. K. Sahu, "Suspended-core holey fiber for evanescent-field sensing," Opt. Eng. **46**(1), 010503 (2007).
18. H. Ebendorff-Heidepriem, S. C. Warren-Smith, and T. M. Monro, "Suspended nanowires: fabrication, design and characterization of fibers with nanoscale cores," Opt. Express **17**(4), 2646–2657 (2009).
19. J. Limpert, F. Stutzki, H.-J. Otto, T. Eidam, C. Jauregui, and A. Tünnermann, "Yb-doped large-pitch fibres: effective single-mode operation based on higher-order mode delocalisation," Light: Sci. Appl. **1**(4), e8 (2012).
20. N. A. Issa and L. Poladian, "Vector wave expansion method for leaky modes of microstructured optical fibers," J. Lightwave Technol. **21**(4), 1005–1012 (2003).
21. B. J. Eggleton, P. S. Westbrook, R. S. Windeler, S. Spälter, and T. A. Strasser, "Grating resonances in air–silica microstructured optical fibers," Opt. Lett. **24**(21), 1460–1462 (1999).
22. S. C. Warren-Smith, G. Nie, E. P. Schartner, L. A. Salamonsen, and T. M. Monro, "Enzyme activity assays within microstructured optical fibers enabled by automated alignment," Biomed. Opt. Express **3**(12), 3304–3313 (2012).
23. E. P. Schartner, L. V. Nguyen, D. Otten, Z. Yu, D. G. Lancaster, H. Ebendorff-Heidepriem, and S. C. Warren-Smith, "Multi-point high temperature optical fiber sensor," *Proc. of SPIE* 11200, 1120038 (30 December 2019).